analytical chemistry

pubs.acs.org/ac
Technical Note

Development of a Semiquantitative Barcode Readout Approach for Paper-Based Analytical Devices (PADs) for Enzymatic H_2O_2 and Glucose Detection

Yanawut Manmana, Shuma Kinugasa, Yuki Hiruta, and Daniel Citterio*

Cite This: Anal. Chem. 2025, 97, 1500−1506
Read Online

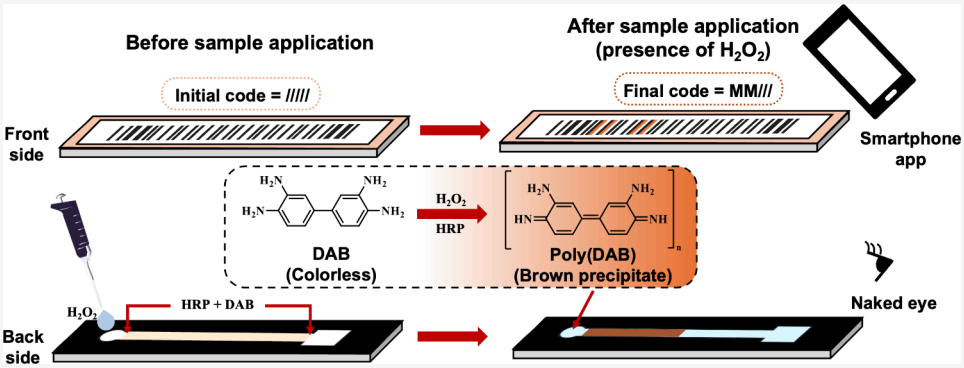

ABSTRACT: The integration of barcode technology with smartphones on paper-based analytical devices (PADs) presents a promising approach to bridging manual detection with digital interpretation and data storage. However, previous studies of 1D barcode approaches have been limited to providing only a "yes/no" response for analyte detection. Herein, a method of using barcode readout for semiquantitative signal detection on PADs has been achieved through the integration of barcode technology with a distance-based measurement concept on PADs. To demonstrate the feasibility of this concept, a PAD fabrication strategy incorporating barcodes was explored, using the enzymatic reaction between horseradish peroxidase (HRP), 3,3′-diaminobenzidine (DAB), and H_2O_2 as a model system. The enzyme-catalyzed polymerization of DAB to polyDAB in the presence of hydrogen peroxide results in the appearance of color observable by the naked eye inside a paperfluidic channel, with the color-changed length depending on the H_2O_2 concentration. At the same time, the barcode pattern displayed as a result of this distance-based color evolution overlaid with a paper-based barcode layer can be read using a smartphone application. Parameters affecting the signal readout performance were studied. The developed device can be used to detect H_2O_2 concentrations in the range of 0.25 to 10 mM within 90 min with 79.6% of barcode signals correctly readable. Additionally, results from different smartphone models showed a consistent reading performance (78.4−79.6%). Finally, the quantification of glucose levels in artificial urine samples was demonstrated. This developed PAD signaling strategy offers end-users more simplicity and can be used as a standalone device or in conjunction with other digital devices.

Addressing global health challenges requires innovative diagnostic tools, particularly point-of-care (POC) testing, which enables rapid in vitro analysis at the patient site. The COVID-19 pandemic highlighted the need for efficient large-scale diagnostics, unattainable with traditional laboratory instruments.[1] Paper-based analytical devices (PADs) have seen explosive growth due to the many attractive characteristics of paper that make it an excellent platform for fabricating POC testing devices. These advantages accelerated the study and development of PADs, targeting various application fields such as medical diagnostics,[2−4] environmental monitoring,[5,6] and food quality monitoring,[7,8] among others.[9−11]

PADs can be applied for both qualitative and quantitative tests. For quantitative assays, the use of colorimetric,[12−14] fluorescence,[15,16] electrochemical,[17,18] and electrochemiluminescence-based[19] signaling methods can be integrated. However, while sensitive quantitative target detection can be achieved, special equipment for readout and quantitative interpretation of the detection signal are usually required. Colorimetry holds great potential as a signal detection technique for PADs. Despite visible color changes, quantitative

Received: August 4, 2024
Revised: November 15, 2024
Accepted: January 6, 2025
Published: January 10, 2025

https://doi.org/10.1021/acs.analchem.4c04113
Anal. Chem. 2025, 97, 1500−1506

colorimetric PAD assays generally rely on software to analyze color intensity, while photos must be captured with a camera. As a solution to this challenge, a variety of innovative quantitative/semiquantitative and equipment-free signal transformation schemes for colorimetry-based PADs have already been proposed, where the analytical signal is transformed into the measurement of color change distance,[20−23] the counting of colored detection zones,[24,25] the measurement of time,[24,26] or the reading of a displayed text.[27,28] Even though they show tremendous potential in research investigations, their application to commercial devices is currently limited.

As an emerging modern technology, barcode technology, which is generally used for data storage and information encoding, has become increasingly used beyond its original field of application. With the increasing availability of smartphones in recent years, barcodes can be readily read without the need for dedicated equipment. Although barcodes as output signals cannot be interpreted by the naked eye, the big advantage of smartphone-assisted readout is the elimination of user-dependent subjective result interpretation.[29] In addition, the output data can be stored or sent to a professional for further data analysis, which cannot be done digitally by other equipment-free strategies. The use of barcodes as a signal readout method for PADs has been reported.[29−32] However, the use of a barcode reading is currently limited to applications in which a "yes/no" answer is sufficient. Therefore, the development of methods or strategies that enable a barcode-based readout of quantitative information remains a challenge. Although the concept of employing barcode-style lateral flow assays for semiquantitative analyte detection has been proposed,[33−35] current implementations still depend on visual interpretation. This is primarily due to prior approaches not making use of a standardized barcode system recognizable by ordinary barcode scanners or by smartphones not equipped with custom-made scanning apps. Our research group previously introduced the use of QR codes in conjunction with a distance-based method for semiquantitative analysis on PADs.[29] However, this approach necessitates multiple QR codes for different concentration levels, thus requiring numerous QR code readings accompanied by certain error risks. Consequently, there is a need for the development of a single-code system for semiquantitative detection on PADs.

In this work, 1D semiquantitative barcode readout with smartphones was studied. A PAD fabrication strategy with a 1D barcode was investigated using the enzymatic reaction of horseradish peroxidase (HRP), 3,3′-diaminobenzidine (DAB), and H_2O_2 as a model system. The polymerization of DAB to polyDAB results in the appearance of color inside a paperfluidic channel, with the color-developed length depending on the H_2O_2 concentration being observable by the naked eye. At the same time, the barcode pattern changes can be read by using a smartphone application. Parameters affecting signal readout performance for both the naked eye distance-based measurement and barcode readout were studied. Finally, glucose detection in artificial urine was performed to demonstrate the possibility of a practically relevant application.

EXPERIMENTAL SECTION

Materials and Instruments. All chemicals were obtained from commercial suppliers and used as received (details are provided in the Supporting Information).

PAD Fabrication. The final PAD design contains two key layers: the barcode layer and the reaction layer. For the barcode layer, the initial code was generated using the Code 39 standard. The barcode pattern was created using Silhouette Studio software (Silhouette, Lindon, UT) and printed using an inkjet printer on label stickers. Then, the sticker paper was cut with Silhouette Cameo 3. The barcode size and width were varied for optimization, and the corresponding parameters are given in the text and figures.

For the reaction layer, Whatman No.1 filter paper was cut into A4 (210 × 297 mm^2) size, followed by printing wax patterns and melting of the wax into the paper on the hot plate (150 °C, 2.5 min). The details of the final printing designs are listed in Figure 1. After wax printing and melting, 5 mg/mL of

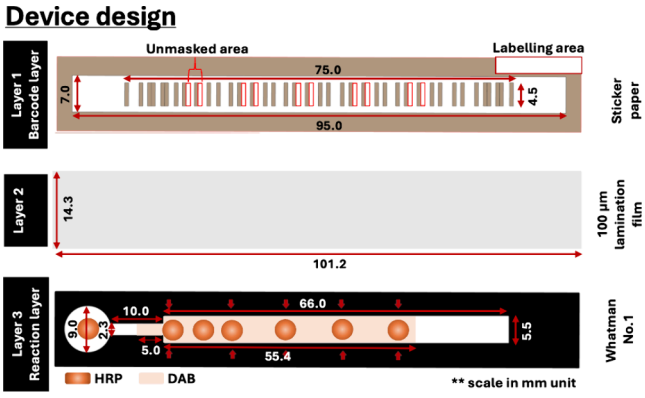

Figure 1. Design of the final device and reagent deposition layout: the brown colored frame and bars in layer 1 are deposited by inkjet printing of standard ink; red framed "unmasked areas" are removed by paper cutting; and black color in layer 3 represents hydrophobic wax.

DAB solution was deposited onto the entire reaction channel through inkjet printing from the black ink cartridge (approximately 4.7 µL; calculation method provided in the Supporting Information and in Figure S1). Then, 0.5 µL of a 5 mg/mL HRP solution was deposited as multiple spots on specific areas of the channel by manual pipetting (Figure 1). After completed reagent deposition, the reaction layer was laminated with the laminator set to 100 °C by attaching the front side (reagent deposited side) to a lamination sheet. After lamination, the reaction layer was attached to the barcode layer directly with the original glue of the sticker paper. A4 sheets of assembled devices were finally cut into single devices for H_2O_2 detection. The schematic overview of the entire PAD fabrication process is shown in Figure S2.

H_2O_2 Detection and Barcode Readout. For H_2O_2 detection, 80 µL of H_2O_2 standard solutions in the range of 0.25−10 mM was added into the sample inlet and the solution allowed to flow until it reached the end of the reaction channel. To maintain a constant humidity, devices were placed in a box with a wetted tissue paper with closed lid for 1 h. Then, the box lid was opened to let the device dry for another 30 min. After the reaction was complete and the device was dried, photos of each device were taken and the color-changed distance was further analyzed by using ImageJ for more precise distance measurement.

The barcode was scanned with the smartphone after the device was flipped over (Figure S3). A similar device fabrication and signal readout procedure was used for glucose detection in artificial urine with some adjustments (details are provided in the Supporting Information).

https://doi.org/10.1021/acs.analchem.4c04113
Anal. Chem. 2025, 97, 1500−1506

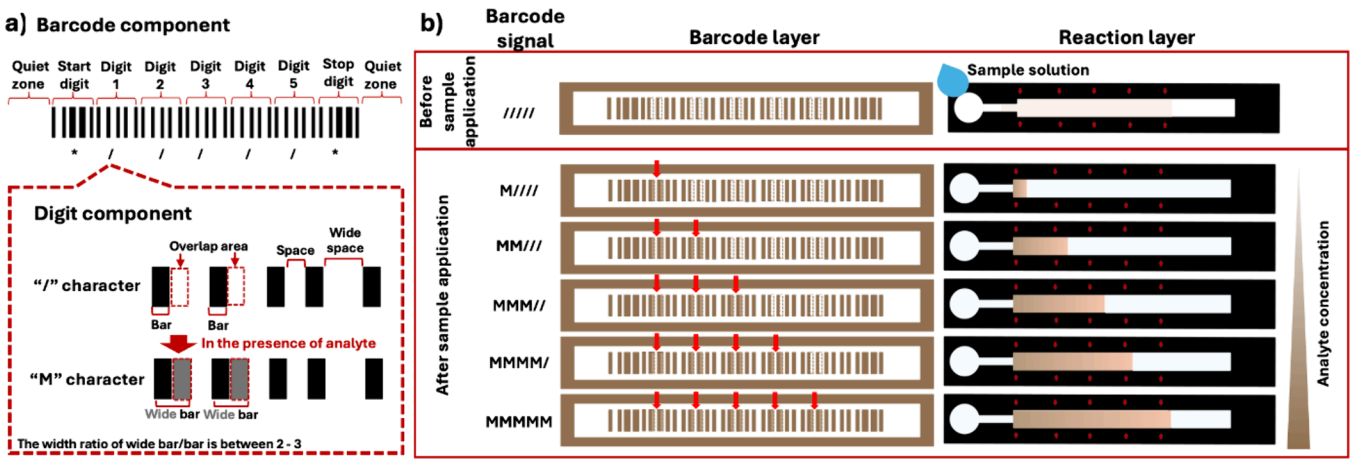

Figure 2. Schematic illustration explaining the principle of quantitative 1D barcode readout PADs: (a) Components of the Code 39 barcode system[36] and signaling principle through analyte-induced conversion of normal bars into wide bars. (b) Combination of distance-based signaling with barcode mask; changes of the barcode pattern depend on the concentration of the target analyte; red arrows indicate bar positions that change from normal to wide state.

Barcode reading was performed with Google Pixel 6 with the barcode scanner application unless mentioned otherwise. The settings for the application are shown in Figure S4. To read the barcode, the paper device was placed on a white A4 paper, and the smartphone was held straight above the device at an angle showing the least reflection from the lamination sheet. The flash from the smartphone was used to reduce the effect of the surrounding light conditions. To investigate the influence of the smartphone models, Redmi Note 11 Pro and iPhone 8 hardware with the same barcode application were used for scanning the same set of devices. The settings on the application were set to be identical to the greatest extent possible (differences in smartphone operating systems).

RESULTS AND DISCUSSION

Principle of Semiquantitative Barcode Readout PADs. The principle applied for semiquantitative barcode readout was inspired by previous work that developed barcodes for the simultaneous detection of multiple drugs of abuse, biomarkers of blood-transmitted infections, drug residues in milk, and nucleic acids.[30,32] In those previous works, a typical Codabar barcode or a new set of barcode patterns was generated as the starting code, which can be changed by immunologic reactions in the presence of target analytes. However, this principle has been applied only for obtaining qualitative results. To expand the application for semiquantitative analysis, the previous concept of barcodes was combined with the idea of equipment-free distance-based signaling previously realized on PADs, wherein a target analyte concentration-dependent change in the length of colored or color-changed sections of a microfluidic channel is observed by the naked eye. In this work, Code 39, another barcode standard system that is commonly used in the industrial field,[36] was used to generate the barcode. Code 39 is named for its pattern, wherein one character is represented by 9 bars and spaces, 3 of the bars/spaces being wider than the others. A typical barcode with the Code 39 standard consists of an asterisk (*) as a start and stop digit, data digits as a message between the start and stop digits, and a quiet zone, as shown in Figure 2a. The bar pattern of each character in Code 39 was studied to identify sets of patterns that show overlap between normal bars and wide bars at the same position. One set of bar patterns that show such overlap can be found in the case of the "/" and "M" characters. Therefore, the set of "/////" characters was set as the initial data message. When depositing colorimetric reagents on the overlapping bar/space positions, the "/" character can change to the "M" character in the presence of target analytes. Based on the distance-based signaling principle overlaid with a barcode pattern featuring transparent unmasked sections (paper cut-outs), a target analyte concentration-dependent number of bars will change from the normal state to the wide state. This results in changes of the barcode signal readout from "/////", "M////", "MM///", ..., to "MMMMM", based on the concentration of the target analyte (Figure 2b). This change in barcode pattern can be scanned using a smartphone application, and the obtained barcode readout can be interpreted back into the target analyte concentration range represented by a particular barcode signal.

For proof-of-concept of semiquantitative barcode readout, H_2O_2 was selected as the model analyte. DAB was used as the colorimetric reagent, which is converted into polyDAB in the enzymatic reaction with HRP in the presence of H_2O_2, leading to a transition from a colorless to a brown color state that can be observed with the naked eye. Since polyDAB has low water solubility, the colored reaction product remains stationary, making DAB an ideal colorimetric reagent for distance-based measurements, as has already been reported.[37−39]

Design of the Barcode Readout PAD and Optimization of the Barcode Layer. The final PAD providing a successful barcode readout was designed by spatially separating the barcode and reaction layers, with the barcode layer being realized as a mask to be placed on top of the reaction layer. Only the areas related to character changes from "/" to "M" were unmasked by cutting (Figure S2). By using the 2-layer masking technique, the DAB reagent can be deposited in a uniform continuous shape. In addition, the two-layer mask approach wherein the barcode layer (Figure 1, layer 1) is separated from the reaction layer (Figure 1, layer 3) by a sheet of lamination film (Figure 1, layer 2) prevents the former from being in contact with the sample liquid, eliminating any washing out effect. To achieve this device design, the precise and reproducible cutting of the unmasked areas of the barcode layer is essential. A Silhouette Cameo 3 cutting tool, equipped

https://doi.org/10.1021/acs.analchem.4c04113
Anal. Chem. 2025, 97, 1500−1506

with an optical sensor, was used. Using its software's "registration marks" function enabled accurate calibration of the cutting area (Figure S5).[40] The cutting performance was investigated using barcodes with varying overall widths (4.5−8.5 cm), widths of the cutout areas (0.45−0.85 mm), and heights of printed bars and cutout areas (1.0−6.0 mm). When measuring the actual dimensions of the cut bar areas, they were found to be approximately 0.2 mm larger in both width and height than the printed bars. Moreover, a decrease in the width of the adjacent printed bar can be observed (Figure S6). For Code 39 recognition, wide bars can have between 2 and 3 times the width of a normal bar. Therefore, for the ideal result, the width of the cut bar and adjacent printed bar should be the same (the cut bar/adjacent printed bar ratio should be close to 1). Based on the cutting precision limits of the cutting tool used in this work, a cut bar width setting above 0.65 mm is needed. For the bar heights, the cutting performance is not a major issue. However, it was found that barcodes cannot be read at bar heights below 1 mm.

Barcode reading with a smartphone camera depends on the contrast between the bars and spaces. To test the general barcode readability, a black base barcode was combined with additional elements of red, blue, green, and yellow colors, and barcode signals were scanned with the smartphone (Figure S7). The combination of a black base barcode with red, blue, and green elements resulted in the transformation of bars from the normal to the wide state, changing the signal readout from "/" to "M" characters. This cannot be achieved with a yellow element addition due to insufficient contrast on a white background. It should be noted that the normal to wide state bar transformation depends not only on the color shade itself but also on the intensity of the specific color. The polymerization of DAB to polyDAB in the presence of H_2O_2 and HRP results in formation of a brownish precipitate. Therefore, model experiments were performed using six base barcodes printed in different color shades ranging from black to brown to light orange (Table S2), laid over paper strips of the six identical colors, simulating the reaction layer. Signal readout was performed for all color combinations. The results show that most combinations of dark colored barcode layers (black, dark brown) with light colored simulated reaction layers fail to induce changes from "/" to "M" characters. On the other hand, barcodes with lighter color intensities (light orange, dark orange, light brown, and mid brown) provided the desired character switching over the entire investigated range of reaction layer colors, with few exceptions. The light brown barcode with the color most similar to the formed polyDAB precipitate was selected as the optimal color for further evaluation.

Optimization of the H_2O_2 Reaction Layer. Although the reaction of DAB for distance-based H_2O_2 measurements has already been reported,[37,39,41] prior devices were designed with very narrow flow channels, which are not suitable for the current barcode scanning approach. Therefore, the optimal design of the reaction layer suitable for barcode readout was investigated. First, the optimal width of the reaction layer's flow channel was studied. Reaction channels with 4.5, 5.5, and 6.5 mm of designed channel width were evaluated. To decrease the initial sample flow speed, channels were partially laminated over a length of 2 cm from the sample inlet (Figure S8a). This fluid speed control is essential to achieving sufficient reaction time for polyDAB formation for the detection of low H_2O_2 concentrations. Narrow reaction channels resulted in more homogeneous color change boundaries compared with wide reaction channels (Figure S8c). This is assumed to be related to the distribution of HRP manually deposited as spots (0.5 μL each) inside the channels. In narrower channels, HRP is expected to cover the entire channel width, while this is not the case for wider channels, resulting in inhomogeneous reagent distribution and coloration. In addition to influencing the visually observed changes in colored distance, the reaction channel width is also of importance for the barcode readout with the barcode layer attached. To prevent black wax from appearing in unmasked barcode areas and negatively influencing the readout, the height of the overlaid barcode pattern should be 1 mm narrower than the underlying reaction channel. Although the clearest color change boundaries were observed with 4.5 mm wide reaction channels, the combination with 3.5 mm high barcode patterns provided unreliable results in barcode readout experiments, in particular for low H_2O_2 concentrations (data not shown). For this reason, 5.5 and 4.5 mm were selected as the optimal reaction channel width and barcode pattern height, respectively.

Next, the amount of DAB and HRP on the reaction channel was optimized to improve the color change intensity and to increase the contrast over the background. Combinations of 5 or 10 mg/mL DAB with 6 or 10 spots of 5 mg/mL HRP were tested (Figure S9a). Higher DAB concentrations resulted in a longer distance of color change but also introduced an unwanted color gradient further downstream at high H_2O_2 levels (Figure S9b). On the other hand, no obvious influence on the length of color change was observed when increasing the number of HRP spots. However, a larger number of HRP spots improved the color homogeneity in the upstream section of the reaction channel (Figure S9b). Hence, as a compromise, a 7 HRP spot arrangement (Figure 1) with one additional spot placed in the upstream channel area was selected as the optimal condition, together with a DAB concentration of 5 mg/mL.

Finally, a slightly modified design of the reaction channel was considered. As mentioned above, a decrease in the initial sample flow speed was found to be important to secure a sufficient reaction time for polyDAB formation at low H_2O_2 concentrations. This was originally achieved by partial lamination of the reaction channel. However, during experiments, it was noticed that the presence of the lamination film caused differences in color and contrast perception that is potentially detrimental to barcode readout. As an alternative method to decrease the initial liquid flow speed, a narrowed channel section upstream of the actual reaction and barcode detection zone was introduced (Figures 1 and S10a). This simple geometrical modification resulted in the final optimized reaction layer design achieving initial liquid flow rates similar to those of the partial lamination approach (Figure S10b), while eliminating the disadvantages associated with the presence of the lamination film.

Barcode Readout H_2O_2 Assay Performance. After optimization of both the barcode and the reaction layers, the overall device performance was tested. Color distance-based H_2O_2 detection was achieved in the range of 0.25−10 mM (Figure 3) with relative standard deviations (RSDs) ranging from 0.56 to 10.83% for interday precision (devices fabricated on 3 different days; Table S3). For the H_2O_2-concentration-dependent barcode readout, the following sets of 5 character signals (/ and M) were expected: 0 mM → /////, 0.25−0.5 mM → M////, 1 mM → MM///, 2 mM → MMM//, 3 mM

https://doi.org/10.1021/acs.analchem.4c04113
Anal. Chem. 2025, 97, 1500−1506

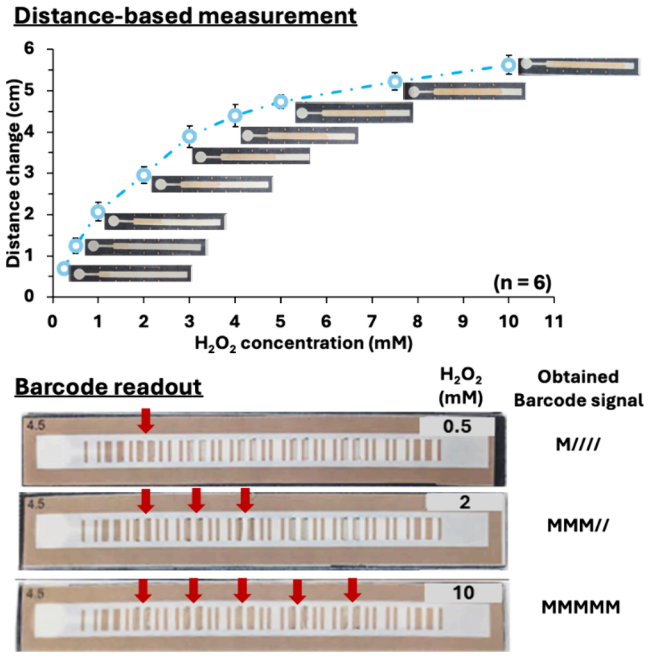

Figure 3. H_2O_2 detection performance with the optimal condition for both distance-based measurement and barcode readout. (For more details, please see Figure S11.)

→ either MMM// or MMMM/, 4−5 mM → either MMMM/ or MMMMM, and 7.5 mM or higher → MMMMM (Figure 3, Figure S11, Table S4). In this experiment, the percentage of correctly readable barcodes was found to be 79.6% among a total of 162 devices and different analyte concentrations (Tables S4 and S5). Although far from being perfect, these results are a promising step toward the use of the developed device in semiquantitative analyte concentration readout with the smartphone-based barcode method for electronic data management and digital result transfer. Causes of barcode scanning errors have been identified in both the barcode layer and the reaction layer (Figure S12). The former one is associated with the limitations in the cutting tool performance during barcode layer fabrication. If the cut paper sections are too narrow, the adjacent printed bar is damaged during the cutting process, or a white (uncut) gap remains between the adjacent printed bar and the unmasked cut area, transitions from a narrow to a wide bar cannot be recognized (Figure S12a). This problem was solved by replacing the imperfect barcode sticker paper with a properly cut version. Errors caused by the signal in the reaction layer are due to variations in the developed color change distance. Switching from a "/" to a "M" character requires the transition of two neighboring bars from the narrow to the wide state. In the case of only one of the bars changing its width (Figure S12b), the pattern cannot be identified, and the entire barcode becomes nonreadable. This challenge is inherent to the used barcodes and cannot be overcome with the Code 39 system. The only possible solution would be the development of a new barcode system encoding different characters through changes of a single bar, similar to a previous report.[32] However, this requires a dedicated barcode readout app, sacrificing the general usability of the system.

The robustness of the barcode readout performance was studied. One of the advantages of barcode readout PADs is their independence of subjective user-interpreted results. To investigate the robustness of this analytical technique, 3 different smartphone models (Google Pixel 6, Redmi Note 11 Pro, and iPhone 8) were used for scanning the identical 3 sets of barcode devices (total of 162 devices). The data summarized in Tables S4 and S5 shows that the total percentages of correctly read barcodes for the Google Pixel 6, Redmi Note 11 Pro, and iPhone 8 smartphones were 79.6, 79.6, and 78.4%, respectively. Most of the barcode devices lead to the same character set readout results with 2 out of the 3 smartphone models tested, and 113 devices provided the same barcode signal for all three smartphone models (69.8%), indicating the robustness of this detection technique. However, the number of devices that result in erroneous readout with more than 2 smartphone models is 29 (17.9%), which is mostly due to changes in the width of only one of two neighboring bars, which is the main challenge of the current approach as also stated above.

Glucose Detection in Artificial Urine. To demonstrate the potential applicability of the developed device to practical samples, we studied the detection of glucose in artificial urine. Glucose oxidase (GOx), catalyzing the oxidation of glucose to produce gluconic acid and H_2O_2, was co-immobilized with HRP. The integration of the additional reaction step of enzymatic conversion of glucose into H_2O_2 by GOx required some modification to the positions for enzyme deposition on the reaction layer. After these adjustments (details in the Supporting Information), the developed device was successfully used for glucose detection in artificial urine samples covering the concentration range between 15 and 200 mg/dL with the following sets of 5 character signals (/ and M) expected: 0 mg/dL → /////, 15 mg/dL → M////, 30 mg/dL → MM///, 50 mg/dL → MMM//, 75 mg/dL → MMMM/, and 150, 200 mg/dL → MMMMM (Figure 4, Figure S13, Table S6). These results serve as an indication of the possibility to apply the developed PAD signaling strategy to practical samples.

CONCLUSIONS

This work demonstrates, to the best of our knowledge, the first semiquantitative 1D barcode readout with smartphones approach implemented on PADs. The colorimetric reaction between H_2O_2, HRP, and DAB was used to demonstrate the proof-of-concept. The semiquantitative barcode readout PADs have been achieved by integrating the concept of distance-based signaling and the barcode principle. With the current device design, results can be obtained either by distance-based naked eye readout or by barcode scanning with smartphones for data storage and further processing. Parameters affecting distance-based signaling and barcode reading performance were studied. Finally, the optimal device can be used to detect H_2O_2 concentrations in the range of 0.25 to 10 mM with 79.6% of correctly readable barcode signals. The satisfactory results obtained from reading the same PAD devices with different smartphone models show the robustness and user-independent character of this detection method. The proof-of-concept demonstration with the H_2O_2 model shows the possibility of adapting this technique for the detection of metabolites in aqueous biological samples by combination with oxidase-family enzymes, as shown by the detection of glucose in artificial urine samples in the range of 15−200 mg/dL. In addition, the device designed with separated barcode and reaction layers allows the conversion of other distance-based detection schemes to barcode readout. Although there are

https://doi.org/10.1021/acs.analchem.4c04113
Anal. Chem. 2025, 97, 1500−1506

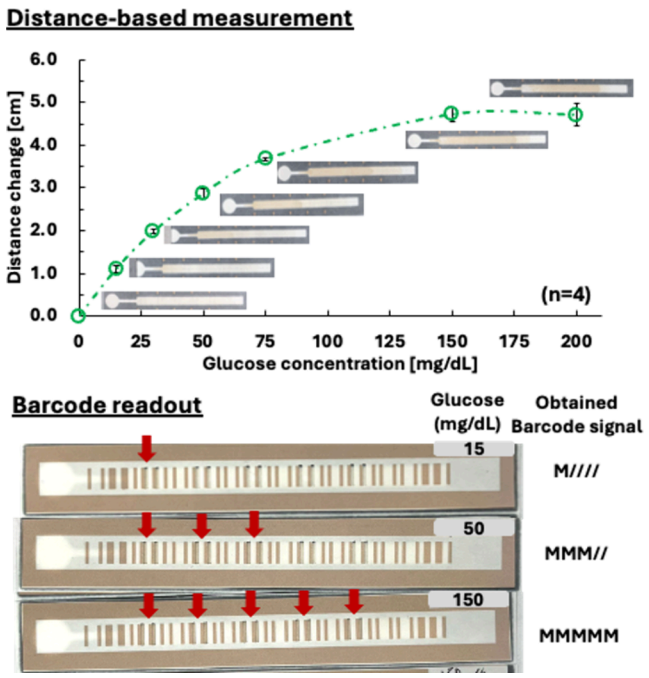

Figure 4. Glucose detection performance in artificial urine for both distance-based measurement and barcode readout. (For more details, please see Figure S13.)

challenges remaining to be solved (long assay time, some errors in barcode scanning), we believe that this prototype of semiquantitative barcode PADs can become a link between analog and digital PAD systems for POC testing.

■ ASSOCIATED CONTENT

Supporting Information

The Supporting Information is available free of charge at https://pubs.acs.org/doi/10.1021/acs.analchem.4c04113.

Reagents and materials; figures illustrating device fabrication, the assay procedure, and the barcode reading app; cutting tool performance; barcode scanning performance for different color combinations; causes of barcode scanning error; and full sets of barcode readout results including use of different smartphone models (PDF)

■ AUTHOR INFORMATION

Corresponding Author

Daniel Citterio − *Department of Applied Chemistry, Keio University, Kohoku-ku, Yokohama 223-8522, Japan;* orcid.org/0000-0001-7420-045X; Phone: +81-45-566-1568; Email: citterio@applc.keio.ac.jp; Fax: +81-45-566-1568

Authors

Yanawut Manmana − *Department of Applied Chemistry, Keio University, Kohoku-ku, Yokohama 223-8522, Japan;* orcid.org/0000-0003-0830-7587

Shuma Kinugasa − *Department of Applied Chemistry, Keio University, Kohoku-ku, Yokohama 223-8522, Japan*

Yuki Hiruta − *Department of Applied Chemistry, Keio University, Kohoku-ku, Yokohama 223-8522, Japan;* orcid.org/0000-0001-7303-4189

Complete contact information is available at: https://pubs.acs.org/10.1021/acs.analchem.4c04113

Author Contributions

The manuscript was written through contributions of all authors. All authors have given approval to the final version of the manuscript.

Notes

The authors declare no competing financial interest.

■ ACKNOWLEDGMENTS

This work was partially supported by a Grant-in-Aid for Research Activity Start-up from the Japan Society for the Promotion of Science (JSPS) (Grant No. 23K19273) to Y. M.

■ ABBREVIATIONS

PADs, paper-based analytical devices; HRP, horseradish peroxidase; DAB, 3,3′-diaminobenzidine; POC, point-of-care; GOx, glucose oxidase

■ REFERENCES

(1) Manmana, Y.; Kubo, T.; Otsuka, K. *TrAC Trends Anal. Chem.* **2021**, *135*, 116160.
(2) Allameh, S.; Rabbani, M. *Appl. Biochem. Biotechnol.* **2022**, *194* (5), 2077−2092.
(3) Liu, C.; Gomez, F. A.; Miao, Y.; Cui, P.; Lee, W. *Talanta* **2019**, *194*, 171−176.
(4) Fakhri, N.; Abarghoei, S.; Dadmehr, M.; Hosseini, M.; Sabahi, H.; Ganjali, M. R. *Spectrochim. Acta Part A Mol. Biomol. Spectrosc.* **2020**, *227*, 117529.
(5) Xiong, X.; Zhang, J.; Wang, Z.; Liu, C.; Xiao, W.; Han, J.; Shi, Q. *BioChip J.* **2020**, *14* (4), 429−437.
(6) Manbohi, A.; Ahmadi, S. H. *Environ. Monit. Assess.* **2022**, *194* (3), 190.
(7) Danchana, K.; Iwasaki, H.; Ochiai, K.; Namba, H.; Kaneta, T. *Microchem. J.* **2022**, *179* (April), 107513.
(8) Jung, Y.; Heo, Y.; Lee, J. J.; Deering, A.; Bae, E. *J. Microbiol. Methods* **2020**, *168*, 105800.
(9) Abdulsattar, J. O.; Hadi, H.; Richardson, S.; Iles, A.; Pamme, N. *Anal. Chim. Acta* **2020**, *1136*, 196−204.
(10) Dias, B. C.; Batista, A. D.; da Silveira Petruci, J. F. *Anal. Chim. Acta* **2021**, *1187*, 339141.
(11) Tsagkaris, A. S.; Migliorelli, D.; Uttl, L.; Filippini, D.; Pulkrabova, J.; Hajslova, J. *Talanta* **2021**, *222*, 121535.
(12) Kudo, H.; Maejima, K.; Hiruta, Y.; Citterio, D. *SLAS Technol.* **2020**, *25* (1), 47−57.
(13) Liu, C.; Miao, Y.; Zhang, X.; Zhang, S.; Zhao, X. *Microchim. Acta* **2020**, *187* (6), 362.
(14) Lewińska, I.; Speichert, M.; Granica, M.; Tymecki, Ł. *Sensors Actuators B Chem.* **2021**, *340*, 129915.
(15) Borse, V.; Srivastava, R. *Sensors Actuators, B Chem.* **2019**, *280*, 24−33.
(16) Ang, C.; Lou, D.; Hu, L.; Chen, W.; Zhu, Y.; Guo, Z.; Gu, N.; Zhang, Y. *Anal. Sci.* **2018**, *34* (10), 1117−1123.
(17) Chen, C.-A.; Yuan, H.; Chen, C.-W.; Chien, Y.-S.; Sheng, W.-H.; Chen, C.-F. *Lab Chip* **2021**, *21* (10), 1908−1915.
(18) Cao, L.; Fang, C.; Zeng, R.; Zhao, X.; Jiang, Y.; Chen, Z. *Biosens. Bioelectron.* **2017**, *92*, 87−94.
(19) Chen, L.; Zhang, C.; Xing, D. *Sensors Actuators, B Chem.* **2016**, *237*, 308−317.
(20) Chen, Y.; Chu, W.; Liu, W.; Guo, X. *Sensors Actuators, B Chem.* **2018**, *260*, 452−459.
(21) Hiraoka, R.; Kuwahara, K.; Wen, Y.-C.; Yen, T.-H.; Hiruta, Y.; Cheng, C.-M.; Citterio, D. *ACS Sensors* **2020**, *5* (4), 1110−1118.
(22) Zhang, L.; Nie, J.; Wang, H.; Yang, J.; Wang, B.; Zhang, Y.; Li, J. *Anal. Methods* **2017**, *9* (22), 3375−3379.
(23) Yamada, K.; Henares, T. G.; Suzuki, K.; Citterio, D. *ACS Appl. Mater. Interfaces* **2015**, *7* (44), 24864−24875.

(24) Lewis, G. G.; DiTucci, M. J.; Phillips, S. T. *Angew. Chemie Int. Ed.* **2012**, *51* (51), 12707−12710.
(25) Zhang, Y.; Gao, D.; Fan, J.; Nie, J.; Le, S.; Zhu, W.; Yang, J.; Li, J. *Biosens. Bioelectron.* **2016**, *78*, 538−546.
(26) Lewis, G. G.; Robbins, J. S.; Phillips, S. T. *Anal. Chem.* **2013**, *85* (21), 10432−10439.
(27) Yamada, K.; Suzuki, K.; Citterio, D. *ACS Sensors* **2017**, *2* (8), 1247−1254.
(28) Misawa, K.; Yamamoto, T.; Hiruta, Y.; Yamazaki, H.; Citterio, D. *ACS Sensors* **2020**, *5* (7), 2076−2085.
(29) Katoh, A.; Maejima, K.; Hiruta, Y.; Citterio, D. *Analyst* **2020**, *145* (18), 6071−6078.
(30) Yang, M.; Zhang, W.; Yang, J.; Hu, B.; Cao, F.; Zheng, W.; Chen, Y.; Jiang, X. *Sci. Adv.* **2017**, *3* (12), No. eaao4862.
(31) Burklund, A.; Saturley-Hall, H. K.; Franchina, F. A.; Hill, J. E.; Zhang, J. X. J. *Biosens. Bioelectron.* **2019**, *128*, 97−103.
(32) Yang, M.; Zhang, W.; Zheng, W.; Cao, F.; Jiang, X. *Lab Chip* **2017**, *17* (22), 3874−3882.
(33) Yin, H.-Y.; Chu, P.-T.; Tsai, W.-C.; Wen, H.-W. *Food Chem.* **2016**, *192*, 934−942.
(34) Contreras Alvarez, L. A.; Lazo Jara, M. D.; Campos, F. V.; de Oliveira, J. P.; Guimarães, M. C. C. *Food Addit. Contam. Part A* **2024**, *41* (4), 424−437.
(35) Leung, W.; Chan, C. P.; Rainer, T. H.; Ip, M.; Cautherley, G. W. H.; Renneberg, R. *J. Immunol. Methods* **2008**, *336* (1), 30−36.
(36) CODE 39 and Codabar. https://www.keyence.com/ss/products/auto_id/codereader/basic/code39.jsp (accessed May 5, 2023).
(37) Wei, X.; Tian, T.; Jia, S.; Zhu, Z.; Ma, Y.; Sun, J.; Lin, Z.; Yang, C. J. *Anal. Chem.* **2016**, *88* (4), 2345−2352.
(38) Chen, C.; Zhao, L.; Zhang, H.; Shen, X.; Zhu, Y.; Chen, H. *Anal. Chem.* **2019**, *91* (8), 5169−5175.
(39) Cate, D. M.; Dungchai, W.; Cunningham, J. C.; Volckens, J.; Henry, C. S. *Lab Chip* **2013**, *13* (12), 2397.
(40) Rahbar, M.; Nesterenko, P. N.; Paull, B.; Macka, M. *Anal. Chem.* **2017**, *89* (22), 11918−11923.
(41) Chen, C.; Zhao, L.; Zhang, H.; Shen, X.; Zhu, Y.; Chen, H. *Anal. Chem.* **2019**, *91* (8), 5169−5175.

https://doi.org/10.1021/acs.analchem.4c04113
Anal. Chem. 2025, 97, 1500−1506